

Highly Efficient and Stable Planar Perovskite Solar Cells with Modulated Diffusion Passivation Toward High Power Conversion Efficiency and Ultrahigh Fill Factor

Long Zhou, Zhenhua Lin, Zhijun Ning, Tao Li, Xing Guo, Jing Ma, Jie Su, Chunfu Zhang, Jincheng Zhang, Shengzhong Liu, Jingjing Chang,* and Yue Hao

2D/3D perovskite heterostructures or composites are recognized as efficient strategies to improve the stability of perovskite solar cells. Herein, a novel solution process to develop 2D/3D perovskites with modulated diffusion passivation by introducing phenylethylammonium iodide (PEAI) and *N,N*-dimethylformamide (DMF) additive, which could effectively enhance device performance and long-term stability, is demonstrated. Compared with conventional devices, the device with PEAi and DMF solvent additive treatment exhibit enhanced charge transport, improved charge extraction, and suppressed non-radiative carrier recombination. The solar cells with an optimal 2D/3D perovskite passivation treatment exhibit an extremely high fill factor of 83.6% and an average power conversion efficiency of 21.4% (21.3% using integrated photocurrent from the incident photon-to-current efficiency spectra) based on the NiO_x hole transport layer. Furthermore, the unencapsulated device exhibits excellent stability under continuously simulated sunlight illumination and outstanding air stability after 1000 h of storage under ambient air conditions.

multicrystalline silicon. However, perovskite materials still have a long way for further industrial applications due to their instability in ambient air. For instance, 3D perovskites (MAPbI₃) showed chemical instability owing to ion migration and the hygroscopicity of organic MA⁺ cations.^[8–10] Moreover, for perovskites, phase transition occurs between the tetragonal and cubic phase in relatively lower temperature and it exhibits low crystallization energy, which results in the instability of perovskites.^[11–13] In addition, oxygen radical formation plays an important role in PSC degradation due to its natural volatility and instability.^[14,15] Recently, significant attention has been paid to improve the stability of PSCs via composition engineering and interface engineering.^[16–18] Moreover, an effective method to suppress trap density and reduce charge recombination in PSCs is to

1. Introduction

Perovskite solar cells (PSCs) have been considered as promising next-generation photovoltaic devices, owing to their good light absorption, tunable band gap, long charge diffusion lengths, and low fabrication costs, which are beneficial to both high efficiency and commercialization for future sustainable energy.^[1–7] To date, the power conversion efficiency (PCE) of PSCs has already exceeded 24%, comparable to the performance of


introduce long-chain or large radius organic cations into 3D perovskites.^[19–22] In general, the framework of 3D perovskites will transform into 2D layer-like crystal structures due to its large cation radius. Furthermore, 2D perovskites exhibit excellent stability because of the stronger cross-linked action between organic cations and the octahedral structure.^[23,24] However, PSCs based on 2D perovskites have been reported with relatively low efficiency (PCE < 13%) due to their low carrier mobility, large band gap, and short charge diffusion length.^[25–27] Thus, it is a

L. Zhou, Dr. Z. Lin, X. Guo, J. Ma, Dr. J. Su, Prof. C. Zhang, Prof. J. Zhang, Prof. J. Chang, Prof. Y. Hao
State Key Discipline Laboratory of Wide Band Gap Semiconductor Technology
Shaanxi Joint Key Laboratory of Graphene
School of Microelectronics
Xidian University
2 South Taibai Road, Xi'an 710071, China
E-mail: jjingchang@xidian.edu.cn

Prof. Z. Ning
School of Physical Science and Technology
Shanghai Tech University
100 Haik Road, Shanghai 201210, China

Prof. T. Li
Centre for Spintronics and Quantum System
State Key Laboratory for Mechanical Behavior of Materials
School of Materials Science and Engineering
Xi'an Jiaotong University
Xi'an, Shaanxi 710049, China

Prof. S. Liu
Key Laboratory of Applied Surface and Colloid Chemistry
National Ministry of Education
Shaanxi Engineering Lab for Advanced Energy Technology
School of Materials Science and Engineering
Shaanxi Normal University
Xi'an 710119, China

 The ORCID identification number(s) for the author(s) of this article can be found under <https://doi.org/10.1002/solr.201900293>.

DOI: 10.1002/solr.201900293

feasible approach to enhance the stability and exhibit high performance simultaneously using 2D/3D perovskite heterostructures. Recently, Docampo and coworkers demonstrated a facile solution-based cation infiltration process to deposit 2D layer-like perovskites on MAPbI₃. They showed that PSCs with a self-assembly of 2D layer-like perovskites on top of MAPbI₃ exhibited improved moisture stability but relatively low efficiency.^[28] In this case, a significant charge transfer barrier exists due to the quantum-confined energy-level structure of 2D perovskites, which hinders device performance. Subsequently, Snaith and coworkers significantly achieved breakthrough for both efficiency and stability of PSCs via 2D/3D heterostructures by introducing butylammonium, and the PSC reached a higher efficiency of 17.5%.^[29] Furthermore, Jen and coworkers fabricated PSC devices based on the mixed cation FA_x phenylethylammonium iodide (FA_xPEAI_{1-x})₂PbI₃ with a higher PCE (17.7%) and exhibited excellent ambient stability. They proposed that the PEA⁺ ions existed at the crystal grain boundaries and could passivate the surface defects to reduce charge recombination, which could efficiently improve film quality and phase stability.^[30] Recently, Lee et al. reported the fabrication of phase-pure formamidinium-lead tri-iodide perovskite films with excellent optoelectronic quality (20.64%) and stability.^[31] Despite the remarkable achievements, the PCE of the best-performing cells based on 2D/3D perovskite heterostructures remains far inferior to exceeding 22% for planar devices due to the large concentration of organic long chains. The possible reason is that the excess 2D perovskites hinder the charge transport process from 3D perovskites to electrodes during charge extraction and collection. Therefore, it is highly necessary and significant to develop a facile approach to achieve a balance between high efficiency and stability for further practical applications via low concentration modification.

Herein, we proposed a novel solution process to fabricate a 2D/3D perovskite heterostructure on top of the 3D MA_{1-y}FA_yPbI_{3-x}Cl_x perovskite by spin coating mixed methylammonium iodide (MAI) and PEAI solutions with low concentrations to form a mixed perovskite active layer. It was found that 2D/3D perovskites could passivate the grain boundaries, which could efficiently improve photovoltaic performance and moisture stability of PSCs.^[32] Furthermore, we proposed a facile method where *N,N'*-dimethylformamide (DMF) as a polar solvent additive was added to the MAI/PEAI solution to assist diffusion passivation. It was thought that DMF could dissolve the top of 3D perovskites which will recrystallize to form 2D/3D perovskite heterostructures with MAI/PEAI solution. As a result, highly efficient and stable PSCs with PCE exceeding 22% and an extremely high fill factor (FF) of 83.6% have been successfully fabricated via a novel three-step spin-coating method. In particular, the PCE of devices with 2D/3D perovskite heterostructures could go up to 91%, after being exposed to air for 1000 h without any encapsulation.

2. Results and Discussion

A novel sequential three-step spin-coating process was used to fabricate the 2D/3D perovskite thin film based on MA_{1-y}FA_yPbI_{3-x}Cl_x with MAI/PEAI (+DMF additive) incorporation which has been

demonstrated in this study. The detailed experimental process is shown in Figure 1a. In this work, thin films were fabricated on the PEDOT:PSS and NiO_x surface, respectively. By spinning the MAI/PEAI solution, the interdiffusion of MAI/PEAI into the top of 3D perovskites can promote the formation of the 2D/3D perovskite heterostructures on the top surface. DMF as an additive can modulate PEA⁺ distribution and self-assembly on the top surface and grain boundaries of 3D MA_{1-y}FA_yPbI_{3-x}Cl_x perovskites due to their distinct diffusivity and van der Waals interactions between cations,^[33,34] as shown in Figure 1b.

When a proper DMF solvent additive was added, it could help the PEAI cation penetrate into the perovskites to form a 2D/3D perovskite heterostructure with uniform distribution. The self-assembled PEAI with the aid of the DMF additive can promote grain boundary passivation, which is beneficial for effective charge transport in mixed 2D/3D perovskite films.^[33] The qualities of the mixed 2D/3D perovskite thin films were investigated by X-ray diffraction (XRD) techniques. Figure 1c shows the XRD patterns of mixed 2D/3D perovskites with different process methods. The intense diffraction peaks of perovskites appeared at 14.1° and 28.4° which correspond to the (110) and (220) typical crystal planes of the tetragonal phase, respectively. It is clear that the diffraction intensity of mixed 2D/3D perovskites was similar with that of 3D perovskites due to the lower concentration of PEAI used, indicating that the incorporation of large organic cations did not alter the crystal phase of the underlayer of the 3D perovskite thin film. To further gain insights into the formation of low-dimensional perovskites, more details were shown in the XRD patterns of mixed perovskites with a higher PEAI concentration (4 mg mL⁻¹), as shown in Figure S1, Supporting Information. Besides the typical peaks, additional peaks could be observed at 5.45°, 10.9°, 16.35°, 21.8°, and 27.3°, corresponding to the (00*l*) (*l* = 2*n*) planes of low-dimensional perovskites ((PEA)₂(MA)_{*m*-1}PbmI_{3*m*+1}). When the film was treated with MAI/PEAI or MAI/PEAI + DMF, the (00*l*) peak could not be seen clearly in XRD patterns due to its lower concentration. However, it is clear that several additional reflections in the film appeared with a relatively higher concentration (4 mg mL⁻¹) treatment, corresponding to the lattice planes of 2D perovskites ((PEA)₂(MA)_{*m*-1}PbmI_{3*m*+1}). In addition, the grazing incidence wide-angle X-ray scattering (GIWAXS) spectrum was performed to clarify perovskites' crystallization, as shown in Figure 1f and Figure S2, S3, Supporting Information. Notably, there is a pimple typical plane of 2D perovskites marked with a red ring, located at *q* = 0.23 Å⁻¹, which was further verified via 1D GIWAXS in Figure S3, Supporting Information. Meanwhile, there is a stronger scattering pattern located at *q* = 1 Å⁻¹, corresponding to the (110) crystal plane of perovskites. More interestingly, various splitting peaks around the typical planes of the tetragonal phase were observed in Figure S3, Supporting Information, which indicated the enhanced crystallinity and stabilized phase with fabrication on the NiO_x substrate.^[10,35] All of these discussions could further verify the formation of mixed 2D/3D perovskites. Furthermore, the GIWAXS patterns of different conditions have been measured with different incidence angles from 0.2° to 2°. Since the X-ray penetration depth increases with increasing the incidence angles, hence, we can obtain some information about the 2D perovskite depth. As shown in Figure S2, Supporting Information, for films treated

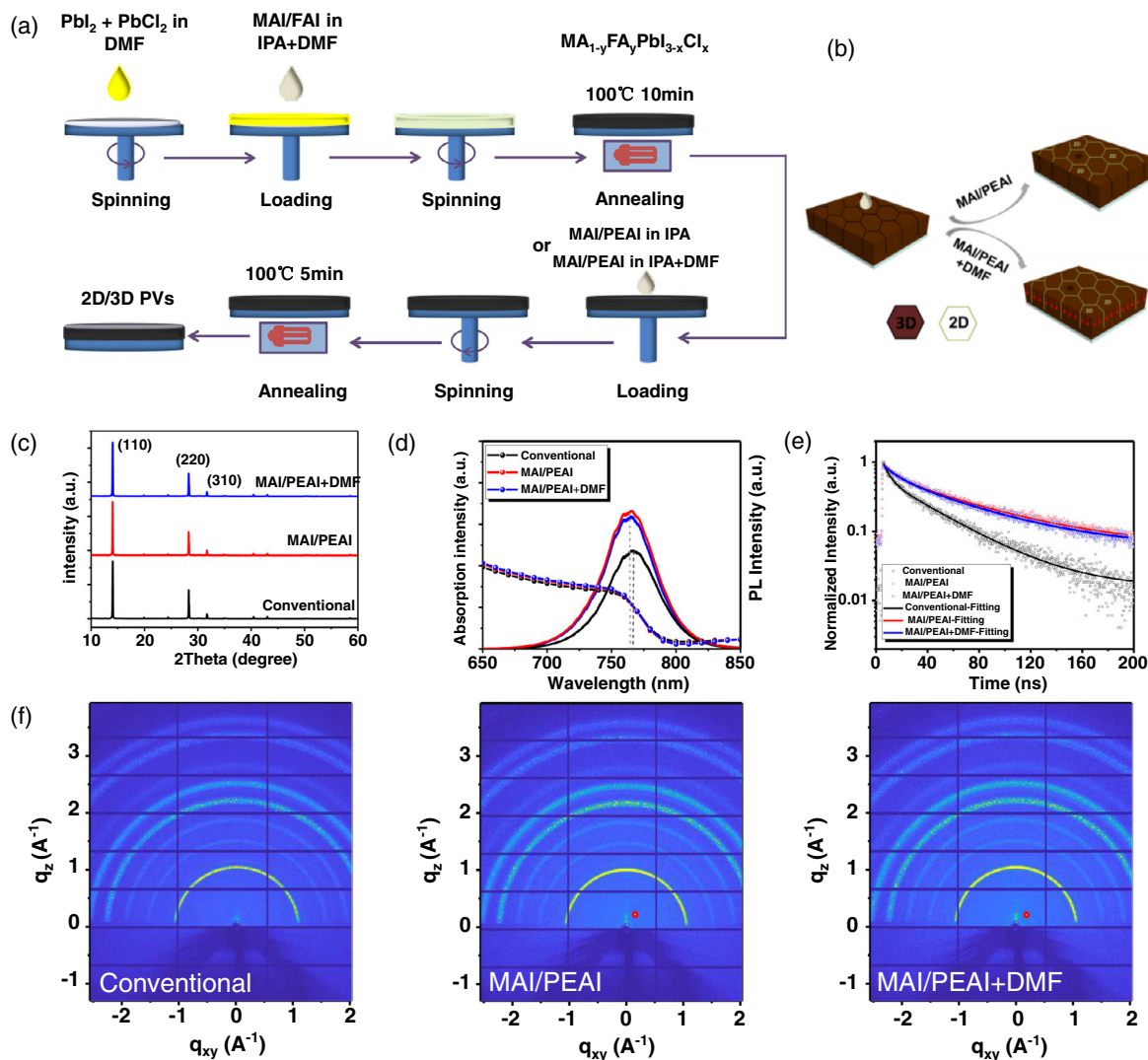


Figure 1. a) Schematic procedure for the preparation of mixed 2D/3D perovskite thin films by a three-step spin-coating method. b) Schematic drawing of perovskites with different treatments. c) XRD patterns of perovskites based on PEDOT:PSS. d) Steady-state PL and absorption spectra of perovskites with different treatments. e) TR-PL of perovskite films with different treatments based on PEDOT:PSS. f) GIWAXS patterns of perovskite films with different treatments.

with MAI/PEAI without the DMF additive, the 2D perovskite peak gradually decreases while increasing the penetration depth, indicating that the 2D perovskite is mainly formed on the surface. While for the film treated with MAI/PEAI with the DMF additive, the 2D perovskite peak shows almost no change, indicating that 2D perovskite undergoes deep diffusion due to the DMF-assisted self-assembly process.

Apparently, there was no peak shift in the XRD pattern, which indicated that the perovskite crystal structure did not change despite the incorporation of PEA^+ cations. Similar results are observed in UV-Vis absorption, as shown in Figure 1d. The passivation treatment and control groups showed a similar absorption profile with an optical band edge around ≈ 790 nm, and the light absorption ability of perovskites with PEA^+ cations was slightly stronger than that of control perovskite films. To further illustrate the quality of perovskite films, the steady-state

photoluminescence (PL) spectra of perovskites on the glass substrates were collected from the perovskite film side, as shown in Figure 1d. With PEAI passivation treatment, we could observe that the peak intensity at 766 nm significantly increased and slightly blue shifted, indicating the improved perovskite film crystallinity and the reduced trap-related nonradiative recombination.^[7] More importantly, to further confirm the formation of low-dimensional perovskites, the PL measurements were performed with wavelength ranging from 520 to 650 nm. It is clear that a small peak appeared at around 564 nm due to the formation of low-dimensional perovskites, as shown in Figure S4, Supporting Information, which is consistent with the large band gap of quasi-2D perovskites.^[36,37] This result could further verify the formation of mixed 2D/3D perovskites. To further confirm the charge carrier dynamics in the mixed perovskite films, the time-resolved PL (TR-PL) decay measurement was carried out

from the air side, as shown in Figure 1e. The carrier lifetimes were extracted from the TR-PL curves with biexponential fitting and the values were listed in Table S1, Supporting Information. It is notable that the average lifetimes of the perovskites with PEAI treatment (60.21 ns for MAI/PEAI, 53.71 ns for MAI/PEAI + DMF) were significantly larger than those of the pristine 3D $\text{MA}_{1-y}\text{FA}_y\text{PbI}_{3-x}\text{Cl}_x$ perovskites (35.45 ns). As laser penetration depth under the excitation wavelength is smaller than perovskite layer thickness, the PL lifetime reflects film quality. A longer PL lifetime after PEAI treatment indicated a reduced nonradiative recombination caused by grain boundaries and crystal defects. Thus, these results showed that the PEAI

passivation treatment could reduce charge recombination in the PSCs. **Figure 2a–d** and **Figure S5**, Supporting Information, showed the morphology of perovskite films with/without PEAI treatment. It is obvious that the laminar crystallized grains could be observed in the scanning electron microscopy (SEM) images of the perovskite film with PEAI treatment due to steric effects of PEA^+ , π -stacking of phenyl rings, and hydrogen bonding interactions between the NH_3^+ -group with the neighboring $[\text{PbI}_6]$ octahedral layer, respectively.^[28] Furthermore, as previous works reported,^[29,32] PEA^+ cations would diffuse into grain boundaries, and the surface morphology would become rough due to the formation of the 2D perovskite film. It is obvious that the laminar

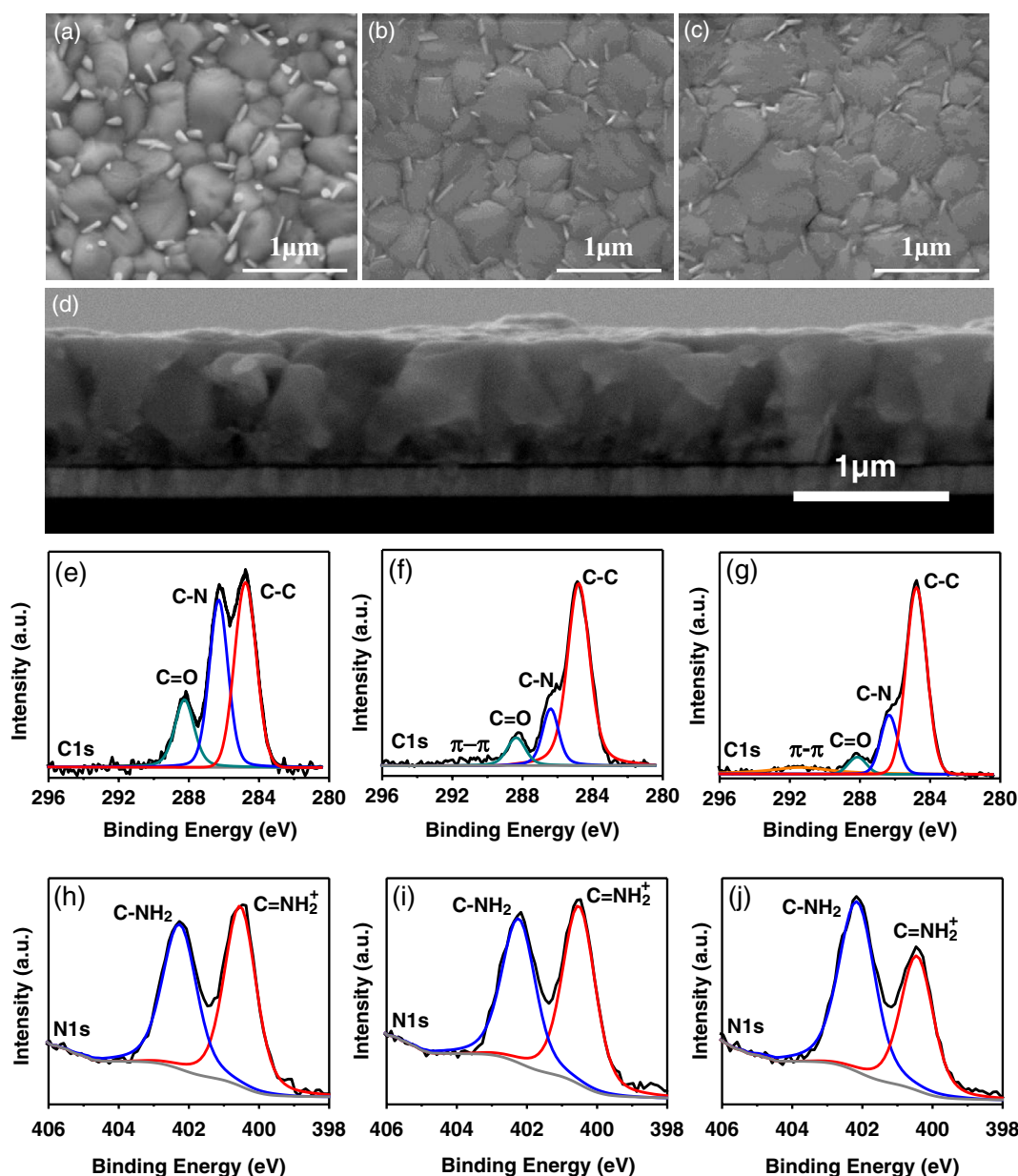


Figure 2. a–d) SEM images of perovskites films: a) 3D perovskites, b) perovskites with PEAI treatment, c) perovskites with PEAI/DMF treatment, and d) cross-section SEM image of perovskites with PEAI/DMF treatment. e–j) XPS spectra of C1s and N1s of perovskites: e,h) 3D perovskites, f,i) perovskites with MAI/PEAI treatment, and g,j) perovskites with MAI/PEAI + DMF treatment.

perovskites existed on the 3D perovskite crystal grains and excess PbI_2 reacted with MAI/PEAI to further form low-dimensional perovskites $((\text{PEA})_2(\text{MA})_{m-1}\text{PbMI}_{3m+1})$, which could further passivate the grain boundaries. Furthermore, similar results in the formation of low-dimensional phases were also verified via atomic force microscopy (AFM) measurements and the step thickness of low-dimensional perovskites determined from the line profile was around 3 nm, as shown in Figure S6, Supporting Information. More interestingly, as shown in Figure 2d and Figure S7, Supporting Information, the addition of DMF could dissolve the top of pristine perovskites and recrystallize with PEAI, which could promote the distribution of 2D/3D perovskite heterostructures uniformly and effective passivation in grain boundaries. Thus, grain boundaries-related charge trapping and recombination could be relieved due to efficient trap passivation and charge transport between crystal grains.

As shown in Figure 2e–j, X-ray photoelectron spectroscopy (XPS) measurements were used to further characterize the formation of the 2D/3D perovskite heterostructure layers. It is clear that the detected C—C (284.8 eV) and C—N (286.5 eV) bonds existed in the C1s spectrum of the pristine 3D perovskite film, corresponding to the presence of FA^+/MA^+ cations. It is unexpected that the emerged C=O bond (288.1 eV) was observed due to decomposition induced by interaction between perovskites and air under ambient conditions during measurement.^[38] Moreover, the typical bonds of C—N and C=N existed in the N1s spectrum of the pristine 3D perovskite film, which was mainly induced by the FA^+ cation. The emerged π — π bond and C—N bond were significantly observed in C1s and N1s XPS spectra of 2D perovskites, corresponding to the incorporation of PEA^+ cations (Figure S8, Supporting Information). It is notable that C=O did not present in the C1s of 2D perovskites, which is consistent with excellent moisture stability. For the XPS spectrum of the mixed 2D/3D perovskites film, the typical peaks of both 3D and 2D perovskites could be observed, indicating the formation of the 2D/3D perovskite heterostructures.

To provide insights into the band alignment between perovskites and transport layers, we have shown the band energy level scheme of different layers in Figure S9, Supporting Information. The band energy level values of NiO_x and perovskites were extracted from ultraviolet photoelectron spectroscopy (UPS) measurements, as shown in Figure S10, Supporting Information. It is noted that the perovskites with MAI/PEAI passivation exhibited smaller work function values (3.93 eV) compared with conventional films (4.31 eV). Moreover, it is clear that the perovskites with MAI/PEAI + DMF passivation exhibited a better band alignment, which would promote charge transfer efficiently to transport layers. Furthermore, the decreased work function could be verified via Kelvin Probe Force Microscopy (KPFM) measurements. It is obvious that the surface potential of conventional perovskite films is much lower than the ones of perovskites with passivation, as shown in Figure S11, Supporting Information.

To assess the PEAI passivation treatment effect on the perovskite film, the PSC devices were fabricated based on a p–i–n-type planar heterojunction architecture using PEDOT:PSS and optimized NiO_x ^[5] as the hole transport layer (HTL). The detailed device fabrication procedures are described in Section 4. The current density – voltage (J – V) characteristics of PSCs with different

conditions are presented in Figure 3a,b. The efficiency distribution performance of PSCs based on different HTLs is shown in Figure 3c,d (Figure S12 and S13, Supporting Information) and summarized in Table 1. Compared with the conventional device, the increased performances of PSCs with PEAI treatment were obtained, indicating the beneficial role of suppressed trap states and charge recombination. Moreover, it is obvious that the DMF as an additive could effectively enhance the performance of PSCs. Both perovskite heterojunction devices provided significantly a higher open-circuit voltage (V_{oc}) (1.02 V for PEDOT:PSS, 1.12 V for NiO_x) than the one composed of pristine 3D perovskite devices (0.95 V for PEDOT:PSS, 1.08 V for NiO_x), which is due to low voltage potential losses ($E_g - qV_{oc}$). It should be mentioned that the FF increased significantly from 78.2% to 80.1% for PEDOT:PSS and from 77.4% to 83.3% for NiO_x after 2D/3D perovskite passivation. It is noted that the short-circuit current density (J_{sc}) of devices based on the DMF additive was slightly higher than the ones with only PEAI, which could be rationalized as the DMF changing the distribution of the 2D/3D perovskite heterostructures to increase charge transport efficiently in the mixed perovskite films. The corresponding steady-state outputs of current density and steady-state efficiency at the maximum power point have been shown in Figure S14, Supporting Information. The reliable devices exhibited steady-state PCE outputs of 16.5%, 17.5%, and 18.1% for devices without and with PEAI (+DMF additive) based on PEDOT:PSS HTL, respectively (Figure S14, Supporting Information). Notably, the devices exhibited steady-state PCE outputs of 19.2%, 20.1%, and 21.3% for devices without and with PEAI (+DMF additive) based on NiO_x HTL, respectively (Figure S14, Supporting Information). All these results were in good agreement with values extracted from their J – V curves, which confirmed the reliability and stability of device performance. The higher J_{sc} values of the perovskites with PEAI treatment and DMF as an additive were obtained due to efficient charge transfer and suppressed charge recombination. Figure S15, Supporting Information, showed the incident photon-to-current efficiency (IPCE) spectra and integrated current density of perovskites with different conditions. The high IPCE value was related with efficient charge transfer and suppressed recombination. The integrated J_{sc} values were consistent with the measured J_{sc} values, which further indicated the reliability of devices.

The best device with perovskites with MAI/PEAI + DMF treatment based on NiO_x HTL showed a high PCE of 22.18% with a J_{sc} of 23.6 mA cm^{-2} , a V_{oc} of 1.12 V, and an extremely high FF of 83.6%, as shown in Figure 4a. The J_{sc} of the best device checked by IPCE spectra is shown in Figure 4b. The J_{sc} (22.8 mA cm^{-2}) of the device was obtained via integrating from the IPCE spectrum and matched well with measured results from the J – V curve (23.6 mA cm^{-2}). Furthermore, the calculated PCE of the best device was 21.3% via using integrated current density from IPCE. Meanwhile, negligible hysteresis could be observed in both forward and reverse scan directions, as shown in Figure 4c. This result could be explained by suppressed interface defects and reduced trap states at grain boundaries, which indicated that perovskites with MAI/PEAI + DMF treatment exhibited efficiently charge carrier transport and suppressed ion migration.^[29] Moreover, Figure 4d shows that the steady-state PCE was measured to be 21.4% for the device based on perovskites with the

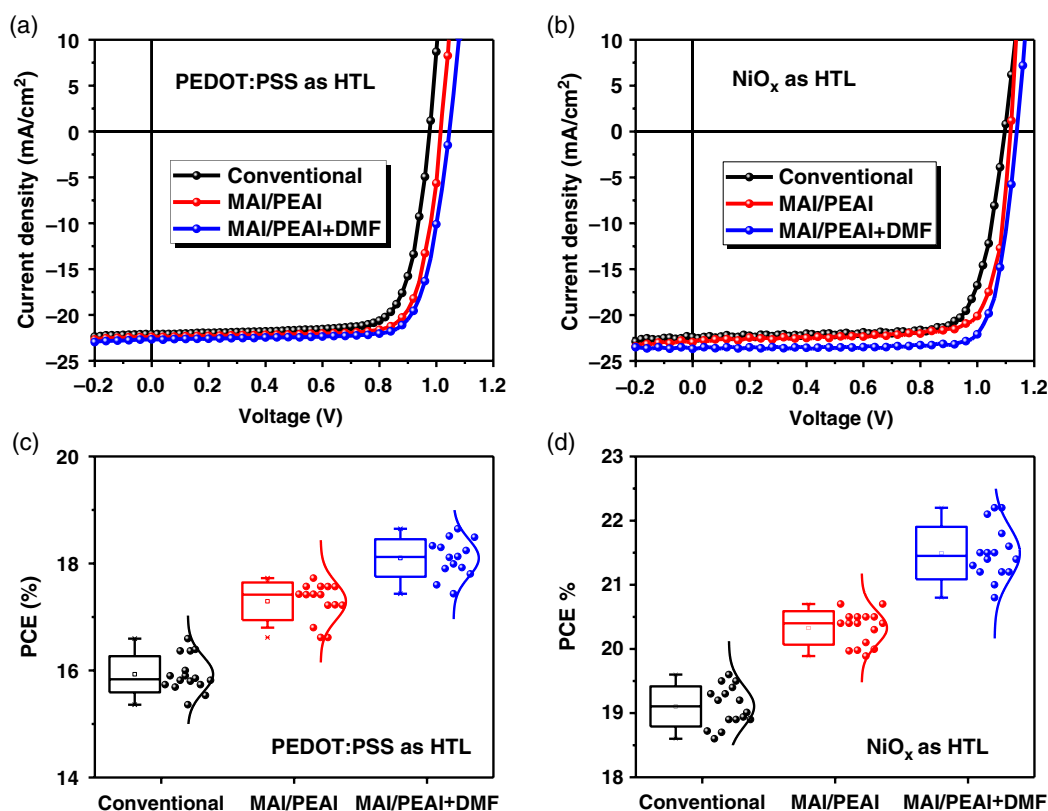


Figure 3. a–b) J - V characteristics of devices with different conditions based on different HTLs: a) PEDOT:PSS as HTL and b) NiO_x as HTL. c,d) Device performance distribution of different conditions with different HTLs: c) PEDOT:PSS as HTL and d) NiO_x as HTL.

Table 1. Summary of the average device parameters for the PSCs with different conditions based on different HTLs. The average results were derived from 96 PSCs.

HTL	Condition	V_{oc} [V]	J_{sc} [mA cm^{-2}]	FF [%]	PCE [%]
PEDOT:PSS	Conventional	0.95	22.09	78.2	16.3
	MAI/PEAI	1.00	22.37	78.4	17.5
	MAI/PEAI + DMF	1.02	22.71	80.1	18.7
NiO_x	Conventional	1.08	22.5	77.4	19.2
	MAI/PEAI	1.10	22.9	80.3	20.3
	MAI/PEAI + DMF	1.12	23.1	83.3	21.4

MAI/PEAI + DMF treatment, and the corresponding current density reached 22.8 mA cm^{-2} . It is clear that photocurrent was quickly stabilized when the light was turned on, which confirmed that there was no hysteresis behavior of the best device.

To confirm the charge transfer and recombination processes of PSCs with PEAI passivation treatment, transient photocurrent (TPC) and transient photovoltage (TPV) were measured. As shown in Figure 5a, the photocurrent decay of perovskite devices with PEAI treatment was faster than the conventional device ($0.95 \mu\text{s}$) and it was found that the device based on perovskites with MAI/PEAI + DMF treatment had a faster decay ($0.72 \mu\text{s}$) than the device based on perovskites with MAI/PEAI treatment ($0.83 \mu\text{s}$), indicating that the device based on perovskites with

PEAI treatment possessed more efficient charge extraction and charge transport processes. Figure 5b shows the results obtained from TPV measurements, which was related with the charge recombination lifetime. It is found that the charge recombination lifetime of devices with PEAI treatment was higher than that of the pristine 3D perovskite devices ($168 \mu\text{s}$). Furthermore, the carrier recombination lifetime of the device with MAI/PEAI + DMF treatment increased to $378 \mu\text{s}$ compared with the device with MAI/PEAI treatment ($323 \mu\text{s}$). Furthermore, we performed the electrical impedance spectroscopy (EIS) measurements to extract the recombination resistance (R_{rec}) and series resistance (R_s) which could confirm the recombination process and charge transport, respectively, in PSCs. The Nyquist plots in the dark condition at an applied voltage of 1 V are shown in Figure 5c and the fitted parameters are listed in Table S2, Supporting Information. The equivalent circuit was composed of R_s , R_{rec} , and a parallel capacitor, in which R_s was related to the high-frequency region and R_{rec} was related to low-frequency region. It is found that the device with mixed 2D/3D perovskites showed a larger R_{rec} and lower R_s , which further verified suppressed carrier recombination and efficient charge transfer. All these results indicated that charge recombination was efficiently suppressed and charge carrier lifetime was enlarged due to the modulated diffusion passivation, which was in good agreement with the results discussed earlier that enhanced film quality and suppressed trap states were obtained in perovskites with additional treatment.

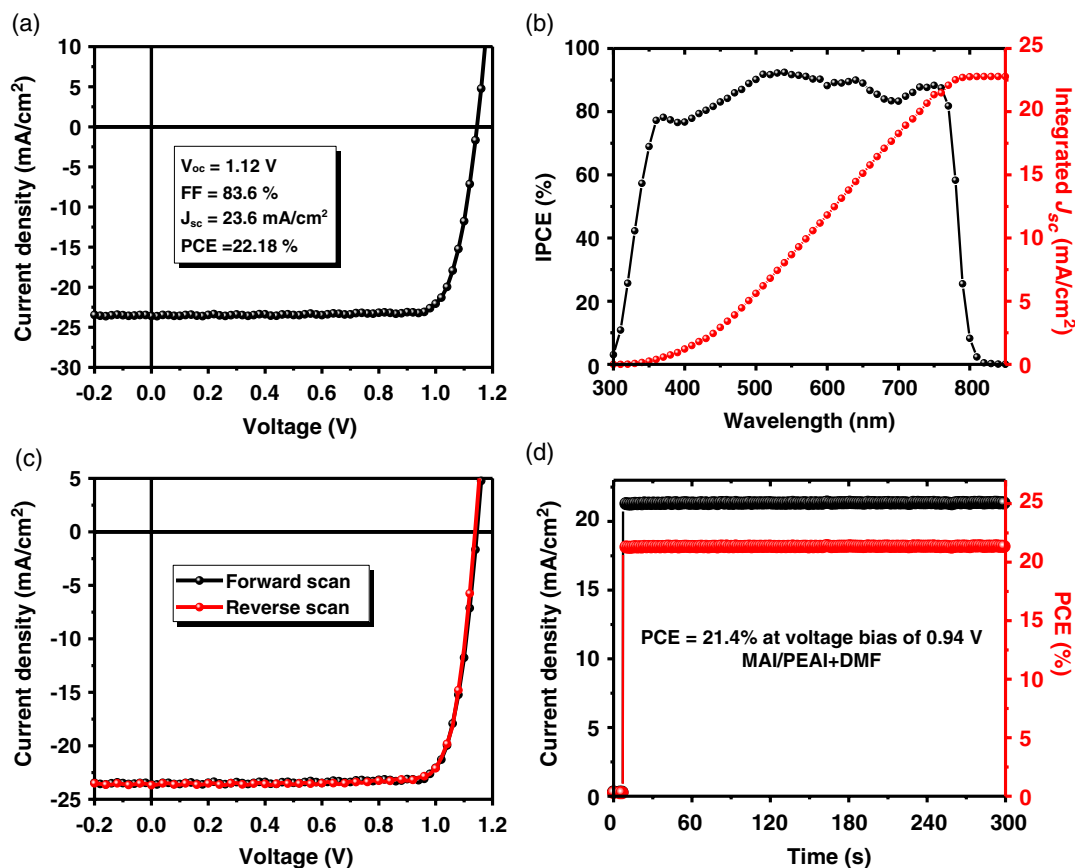


Figure 4. Device performance of the best device for perovskites with MAI/PEAI + DMF treatment based on NiO_x as HTL: a) J–V curve; b) IPCE spectra; c) J–V hysteresis curves; d) Steady-state output of current density and PCE at the maximum power point.

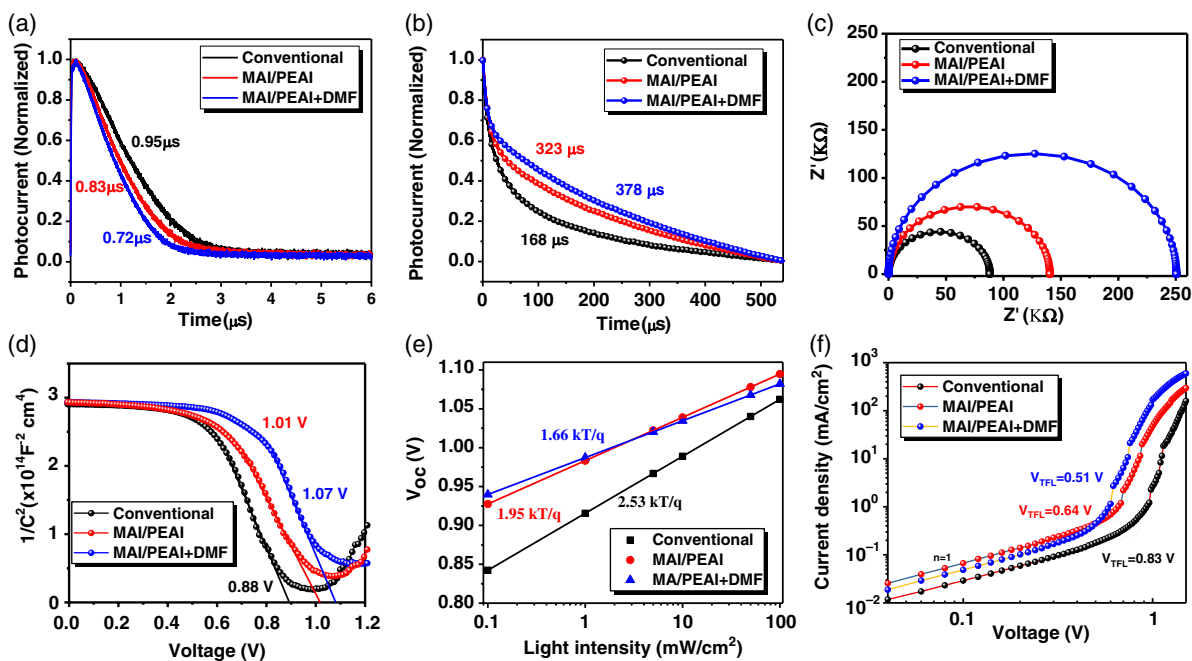


Figure 5. a) TPC and b) TPV measurements; c) Nyquist plots of PSCs with different conditions; d) C–V measurements of perovskite solar cells; e) V_{oc} as a function of light intensity; f) and C–V curves for electron-only devices with different conditions.

To further investigate the effect of the perovskites with PEAI treatment and DMF as additive on device performance, the capacitance–voltage (C – V) characteristics of devices with different treatment conditions were performed to illustrate V_{oc} improvement. The built-in potential (V_{bi}) played an important role in exploring the increased V_{oc} and it could be extracted via the C – V curves according to the Mott–Schottky^[39] relationship, $C^{-2} = 2(V_{bi} - V)/(A^2 q \epsilon \epsilon_0 N)$, where V_{bi} is the built-in potential, V is the applied voltage, A is device active area, ϵ is the relative dielectric constant of the perovskites, ϵ_0 is the permittivity of vacuum, and N is assumed as the doping density of perovskites. The significantly increased V_{bi} (1.01 and 1.07 V for MAI/PEAI and MAI/PEAI + DMF conditions, respectively) compared with that of pristine 3D perovskites (0.88 V) indicated that the perovskites with MAI/PEAI treatment could efficiently promote photogenerated charge carrier separation, charge carrier transport, and extraction (Figure 5d). To further investigate the charge recombination mechanism, V_{oc} was measured with respect to light intensity at various light intensities, from 100 to 0.1 mW cm⁻². As shown in Figure 5e, there was a linear relationship between V_{oc} and light intensity on a semilogarithmic scale with a slope of $nk_B T/q$, where q is elementary charge, k_B is Boltzmann constant, and T is absolute temperature.^[40] The slopes extracted from the fitting curves were 2.53, 1.95, and 1.66 for the control device, the device with MAI/PEAI treatment, and device with MAI/PEAI + DMF treatment, respectively. A higher slope value than $k_B T/q$ indicated that additional trap-assisted recombination existed in PSCs. Thus, a smaller slope value was obtained for the devices after PEAI passivation treatment, which further confirmed a decreased grain boundary-related trap density and charge recombination. Moreover, trap density was determined from the trap-filled limit voltage (V_{TFL}) according to the definition^[41] $V_{TFL} = \frac{e n_{trap} L^2}{2 \epsilon_0 \epsilon}$, where e is the electron charge and L is the thickness of the electron-only device, as shown in Figure 5f. The bias voltage exceeding V_{TFL} indicated that all the traps were filled. Perovskites with PEAI passivation treatment exhibited lower V_{TFL} (0.64 and 0.51 V for MAI/PEAI without and with DMF additive, respectively) compared with pristine 3D perovskites (0.83 V), which indicated reduced electron trap density (1.28×10^{15} and 1.02×10^{15} cm⁻³ for MAI/PEAI without and with DMF additive, respectively) compared with pristine 3D perovskites (1.66×10^{15} cm⁻³). This further confirmed that DMF as additive could recrystallize the perovskites and promote PEAI deeper penetration into perovskites perpendicularly oriented within the pristine 3D perovskite and passivate the trap states more efficiently. Similar results could be confirmed by the steady-state PL and TR-PL.

To investigate the operational and moisture stability of the devices, we measured the unencapsulated devices for 120 min under continuous light illumination with constant AM 1.5 G-illumination without excluding UV light or under ambient air with RH% \approx 50% for 1000 h without excluding room light. As shown in Figure 6a,b, it is demonstrated that the PCEs of devices with PEAI passivation based on different HTLs had high values under continuous illumination in ambient air, and the PCE decrease of devices based on PEDOT:PSS HTL was mainly caused by a slightly decreased J_{sc} and FF. It is expected that

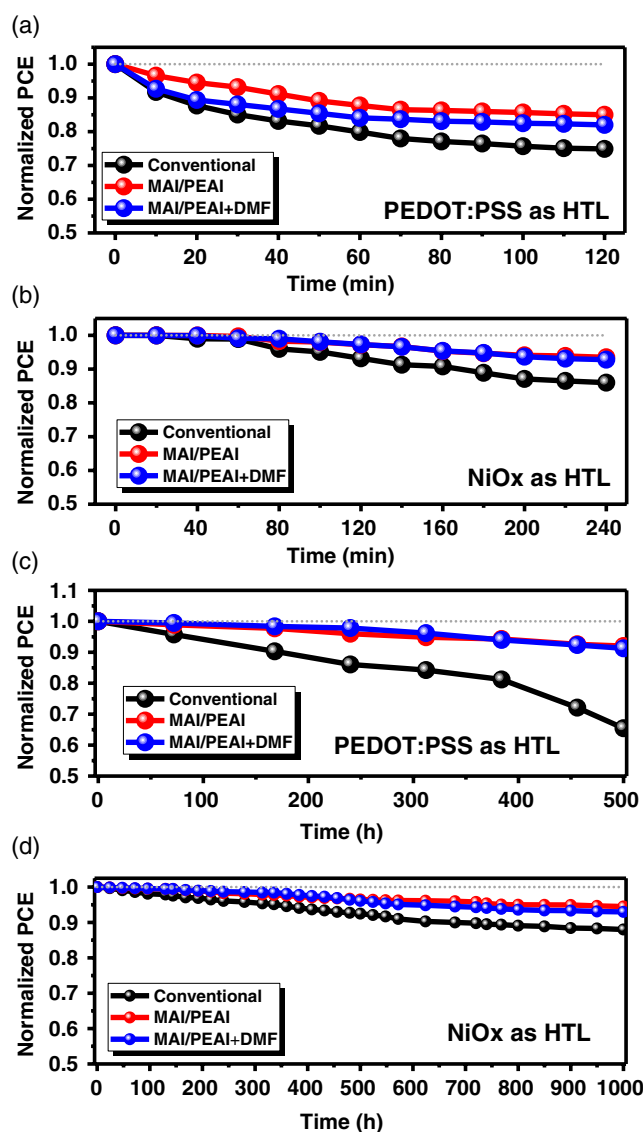


Figure 6. a–b) Illumination stability of devices based on different HTLs: a) PEDOT:PSS as HTL; b) NiO_x as HTL. c,d) Moisture stability of devices based on different HTLs: c) PEDOT:PSS as HTL; d) NiO_x as HTL.

the devices based on NiO_x HTL showed a better light stress stability without obvious PCE decay due to the reduced trap states of the NiO_x or interface between NiO_x and perovskites.^[5] For shelf-life stability, notably, the PCE of mixed 2D/3D perovskite devices without encapsulation was more than 94.5% (MAI/PEAI) and 93.0% (MAI/PEAI + DMF) of their initial values after storage for 1000 h in ambient air. Even for the devices based on PEDOT:PSS HTL, the PCE still was more than 92.0% (MAI/PEAI) and 91.2% (MAI/PEAI + DMF) of their initial values after storage for 500 h in ambient air, as shown in Figure 6c,d. In comparison, the PCEs deteriorated to around 65.4% and 88.1% based on PEDOT:PSS and NiO_x HTL, respectively, for pristine 3D perovskite-based devices. It should be noted that the devices based on perovskites with MAI/PEAI treatment could significantly improve device stability due to the full coverage of 2D perovskites

on pristine 3D perovskites to prevent the penetration of water molecules from the surface into the bulk. However, this also affected the efficient charge carrier transport and decreased the device's current density and PCE. Therefore, to achieve a balance between efficiency and stability, using the DMF additive to modulate passivation behavior is desirable. Anyway, the enhanced stability of passivated devices was related to improved perovskite film quality and beneficial 2D passivation which protected the 3D perovskite from moisture due to the hydrophobic nature of PEA1. Our results demonstrated that the devices with PEA1-treated perovskites exhibited better operation and moisture stability for promising commercialization potentials.

3. Conclusion

In conclusion, we have demonstrated a novel strategy to improve the efficiency and stability of 2D/3D perovskite films with modulated diffusion passivation by introducing PEA1 and DMF as an additive. The DMF solvent additive could promote PEA1 to penetrate into perovskites to form an optimal 2D/3D perovskite heterostructure, which is beneficial for passivating the trap states and enhancing charge transport. As a result, the PSCs based on 2D/3D perovskite films showed significantly improved efficiency and stability. Moreover, we demonstrated that photovoltaic solar cells with the DMF additive based on NiO_x as the HTL reached a high PCE of up to 22.18% (21.3% using integrated photocurrent from the IPCE spectra) due to a significantly increased V_{oc} and FF. The significantly enhanced device performance is contributed by effective charge transport and low charge recombination. Our findings provide a facile strategy to improve both device stability and photovoltaic performance of PSCs for commercial applications.

4. Experimental Section

Materials: All materials, such as methylammonium iodide (MAI, 99.8%, Dyesol), formamidinium iodide (FAI, 99.9%, Dyesol), lead iodide (PbI_2 , 99.999%, Sigma), lead chloride (PbCl_2 , 99.999%, Sigma), 2-phenylethylamine hydroiodide (PEA1, 98.0%, TCI) phenyl-C61-butyl acid methyl ester (PCBM, 98%, nano-c), nickel nitrate ($\text{Ni}(\text{NO}_3)_2 \cdot 6\text{H}_2\text{O}$, 97%, Sigma), DMF (99.8%, Aladdin), PEDOT:PSS (Clevios PVP Al 4083), and bathochroine (96%, Alfa), were used in this work without further purification.

2D/3D Perovskite Film Deposition: For the deposition of mixed 2D/3D perovskite film on NiO_x thin film or PEDOT:PSS, the perovskite precursor solution was first prepared. PbI_2 and PbCl_2 were dissolved in DMF and stirred all night at 65 °C. MAI and FAI at 7:3 of 100 mg were dissolved in the solvent of IPA with 0.9 vol% DMF. The solution of PbI_2 and PbCl_2 (1.36 and 0.24 M) was spin coated at 3000 rpm for 45 s. Then, MAI solution was spin coated on top of the dried PbI_2 layer and annealed at 100 °C for 10 min. After that, the solution of MAI (1 mg) and PEA1 (2 mg) dissolved in IPA (1 mL) with or without 1 vol% DMF and was spin coated on the perovskite film and annealed at 100 °C for 5 min.

Film Formation and Device Fabrication: The indium tin oxide (ITO) glass substrates ($10 \Omega \text{ sq}^{-1}$) were cleaned by ultrasonic treatment with detergent, deionized water, acetone, and ethyl alcohol for 20 min and dried with nitrogen. Then, the ITO substrates were treated with UV–ozone for 20 min to remove organic residues. NiO_x thin film was prepared according to our previous work.^[5] A thin film of NiO_x was spin coated on the ITO glass substrates at 3000 rpm for 45 s and annealed on a hot plate at 250 °C for 45 min as the HTL. The perovskite film as the absorber layer was spin coated on the NiO_x layer using the method discussed earlier. After that,

PCBM (20 mg mL^{-1} in chlorobenzene) as the electron transport layer was spin coated at 2000 rpm for 45 s. Next, a thin layer of BCP (0.5 mg mL^{-1} in IPA) was spin coated on the top of the PCBM layer at 6000 rpm for 45 s. Finally, 100 nm Ag electrode was thermally deposited to finish device fabrication. All the devices had an effective area of 7.5 mm^2 defined by the metal shadow mask.

Materials and Device Characterization: All the devices were measured via Keithley 2400 under the standard solar simulator with an intensity of 100 mW cm^{-2} . The system was calibrated against an National Renewable Energy Laboratory (NREL)-certified silicon reference solar cell. All the measurements of the solar cells were performed under ambient atmosphere at room temperature without encapsulation. IPCE measurements were carried out by the SCS10-X150 systems (Zolix instrument. Co. Ltd). XRD measurements were performed by Bruker D8 Advance XRD. The UV–Vis absorption spectra were measured with the Perkin-Elmer Lambda 950 spectrophotometer. PL and TR-PL spectra were recorded using the Pico Quant Fluotime 300 with a 510 nm picosecond pulsed laser. The morphology characterization of the films was measured by SEM (JSM-7800F). XPS measurements were performed by the Escalab 250Xi with a source of monochromatic Al-Ka (1486.6 eV). TPC measurement was performed with a system excited by a 532 nm (1000 Hz, 3.2 ns) pulse laser. TPV measurement was performed with the same system excited by a 405 nm (50 Hz, 20 ms) pulse laser. A digital oscilloscope (Tektronix, D4105) was used to record the photocurrent or photovoltage decay process with a sampling resistor of 50 Ω or 1 M Ω , respectively.

Supporting Information

Supporting Information is available from the Wiley Online Library or from the author.

Acknowledgements

This work was financially supported by National Natural Science Foundation of China (61604119, 61704131, and 61804111), Natural Science Foundation of Shaanxi Province (2017JQ6002, 2017JQ6031), Fund of the State Key Laboratory of Solidification Processing in NWPU (Grant SKLSP201804, SKLSP201916), and Young Elite Scientists Sponsorship Program by CAST (2016QNRC001).

Conflict of Interest

The authors declare no conflict of interest.

Keywords

2D/3D perovskites, high efficiencies, passivation, perovskite solar cells

Received: July 2, 2019

Revised: August 8, 2019

Published online: August 20, 2019

- [1] M. M. Lee, J. Teuscher, T. Miyasaka, T. N. Murakami, H. J. Snaith, *Science* **2012**, *338*, 643.
- [2] J. Burschka, N. Pellet, S.-J. Moon, R. Humphry-Baker, P. Gao, M. K. Nazeeruddin, M. Grätzel, *Nature* **2013**, *499*, 316.
- [3] D. P. McMeekin, G. Sadoughi, W. Rehman, G. E. Eperon, M. Saliba, M. T. Horantner, A. Haghighirad, N. Sakai, L. Korte, B. Rech, M. B. Johnston, L. M. Herz, H. J. Snaith, *Science* **2016**, *351*, 151.
- [4] W. S. Yang, B.-W. Park, E. H. Jung, N. J. Jeon, Y. C. Kim, D. U. Lee, S. S. Shin, J. Seo, E. K. Kim, J. H. Noh, S. Il Seok, *Science* **2017**, *356*, 1376.

- [5] Z. Liu, J. Chang, Z. Lin, L. Zhou, Z. Yang, D. Chen, C. Zhang, S. F. Liu, Y. Hao, *Adv. Energy Mater.* **2018**, *8*, 1703432.
- [6] L. Zhou, J. Chang, Z. Liu, X. Sun, Z. Lin, D. Chen, C. Zhang, J. Zhang, Y. Hao, *Nanoscale* **2018**, *10*, 3053.
- [7] J. Chang, H. Zhu, B. Li, F. H. Isikgor, Y. Hao, Q. Xu, J. Ouyang, *J. Mater. Chem. A* **2016**, *4*, 887.
- [8] J. A. Christians, P. A. Miranda Herrera, P. V. Kamat, *J. Am. Chem. Soc.* **2015**, *137*, 1530.
- [9] Z. Song, A. Abate, S. C. Waththage, G. K. Liyanage, A. B. Phillips, U. Steiner, M. Graetzel, M. J. Heben, *Adv. Energy Mater.* **2016**, *6*, 1600846.
- [10] W. Nie, H. Tsai, J.-C. Blancon, F. Liu, C. C. Stoumpos, B. Traore, M. Kepenekian, O. Durand, C. Katan, S. Tretiak, J. Crochet, P. M. Ajayan, M. Kanatzidis, J. Even, A. D. Mohite, *Adv. Mater.* **2018**, *30*, 1703879.
- [11] Q. Lin, A. Armin, P. L. Burn, P. Meredith, *Acc. Chem. Res.* **2016**, *49*, 545.
- [12] A. R. Srimath Kandada, A. Petrozza, *Acc. Chem. Res.* **2016**, *49*, 536.
- [13] B. Wu, H. T. Nguyen, Z. Ku, G. Han, D. Giovanni, N. Mathews, H. J. Fan, T. C. Sum, *Adv. Energy Mater.* **2016**, *6*, 1600551.
- [14] A. J. Pearson, G. E. Eperon, P. E. Hopkinson, S. N. Habisreutinger, J. T. W. Wang, H. J. Snaith, N. C. Greenham, *Adv. Energy Mater.* **2016**, *6*, 1600014.
- [15] N. Aristidou, I. Sanchez-Molina, T. Chotchuangchutchaval, M. Brown, L. Martinez, T. Rath, S. A. Haque, *Angew. Chem. Int. Ed.* **2015**, *54*, 8208.
- [16] M. Lyu, J.-H. Yun, P. Chen, M. Hao, L. Wang, *Adv. Energy Mater.* **2017**, *7*, 1602512.
- [17] Y. Hu, F. Bai, X. Liu, Q. Ji, X. Miao, T. Qiu, S. Zhang, *ACS Energy Lett.* **2017**, *2*, 2219.
- [18] T. C. Jellicoe, J. M. Richter, H. F. J. Glass, M. Tabachnyk, R. Brady, S. E. Dutton, A. Rao, R. H. Friend, D. Credgington, N. C. Greenham, M. L. Böhm, *J. Am. Chem. Soc.* **2016**, *138*, 2941.
- [19] T. Zhao, C.-C. Chueh, Q. Chen, A. Rajagopal, A. K.-Y. Jen, *ACS Energy Lett.* **2016**, *1*, 757.
- [20] M. Yuan, L. N. Quan, R. Comin, G. Walters, R. Sabatini, O. Voznyy, S. Hoogland, Y. Zhao, E. M. Beauregard, P. Kanjanaboos, Z. Lu, D. H. Kim, E. H. Sargent, *Nat. Nanotechnol.* **2016**, *11*, 872.
- [21] Z. Xiao, R. A. Kerner, L. Zhao, N. L. Tran, K. M. Lee, T.-W. Koh, G. D. Scholes, B. P. Rand, *Nat. Photonics* **2017**, *11*, 108.
- [22] R. L. Milot, R. J. Sutton, G. E. Eperon, A. A. Haghighirad, J. Martinez Hardigree, L. Miranda, H. J. Snaith, M. B. Johnston, L. M. Herz, *Nano Lett.* **2016**, *16*, 7001.
- [23] B. Saparov, D. B. Mitzi, *Chem. Rev.* **2016**, *116*, 4558.
- [24] D. B. Mitzi, *J. Chem. Soc. Dalton Trans.* **2001**, *13*, 3283.
- [25] H. Tsai, W. Nie, J.-C. Blancon, C. C. Stoumpos, R. Asadpour, B. Harutyunyan, A. J. Neukirch, R. Verduzco, J. J. Crochet, S. Tretiak, L. Pedesseau, J. Even, M. A. Alam, G. Gupta, J. Lou, P. M. Ajayan, M. J. Bedzyk, M. G. Kanatzidis, A. D. Mohite, *Nature* **2016**, *536*, 312.
- [26] D. H. Cao, C. C. Stoumpos, T. Yokoyama, J. L. Logsdon, T.-B. Song, O. K. Farha, M. R. Wasielewski, J. T. Hupp, M. G. Kanatzidis, *ACS Energy Lett.* **2017**, *2*, 982.
- [27] Y. Liao, H. Liu, W. Zhou, D. Yang, Y. Shang, Z. Shi, B. Li, X. Jiang, L. Zhang, L. N. Quan, R. Quintero-Bermudez, B. R. Sutherland, Q. Mi, E. H. Sargent, Z. Ning, *J. Am. Chem. Soc.* **2017**, *139*, 6693.
- [28] Y. Hu, J. Schlipf, M. Wussler, M. L. Petrus, W. Jaegermann, T. Bein, P. Müller-Buschbaum, P. Docampo, *ACS Nano* **2016**, *10*, 5999.
- [29] Z. Wang, Q. Lin, F. P. Chmiel, N. Sakai, L. M. Herz, H. J. Snaith, *Nat. Energy* **2017**, *2*, 17135.
- [30] N. Li, Z. Zhu, C.-C. Chueh, H. Liu, B. Peng, A. Petrone, X. Li, L. Wang, A. K.-Y. Jen, *Adv. Energy Mater.* **2017**, *7*, 1601307.
- [31] J.-W. Lee, Z. Dai, T.-H. Han, C. Choi, S.-Y. Chang, S.-J. Lee, N. De Marco, H. Zhao, P. Sun, Y. Huang, Y. Yang, *Nat. Commun.* **2018**, *9*, 3021.
- [32] Y. Lin, Y. Bai, Y. Fang, Z. Chen, S. Yang, X. Zheng, S. Tang, Y. Liu, J. Zhao, J. Huang, *J. Phys. Chem. Lett.* **2018**, *9*, 654.
- [33] D. H. Cao, C. C. Stoumpos, O. K. Farha, J. T. Hupp, M. G. Kanatzidis, *J. Am. Chem. Soc.* **2015**, *137*, 7843.
- [34] T. M. Koh, V. Shanmugam, J. Schlipf, L. Oesinghaus, P. Müller-Buschbaum, N. Ramakrishnan, V. Swamy, N. Mathews, P. P. Boix, S. G. Mhaisalkar, *Adv. Mater.* **2016**, *28*, 3653.
- [35] S. Wang, B. Zhang, D. Feng, Z. Lin, J. Zhang, Y. Hao, X. Fan, J. Chang, *J. Mater. Chem. C* **2019**, *7*, 9270.
- [36] X. Gan, O. Wang, K. Liu, X. Du, L. Guo, H. Liu, *Sol. Energy Mater. Sol. Cells* **2017**, *162*, 93.
- [37] Y. Cho, A. M. Soufiani, J. S. Yun, J. Kim, D. S. Lee, J. Seidel, X. Deng, M. A. Green, S. Huang, A. W. Y. Ho-Baillie, *Adv. Energy Mater.* **2018**, *8*, 1703392.
- [38] P. Chen, Y. Bai, S. Wang, M. Lyu, J.-H. Yun, L. Wang, *Adv. Funct. Mater.* **2018**, *28*, 1706923.
- [39] Y. Li, L. Meng, Y. Yang, G. Xu, Z. Hong, Q. Chen, J. You, G. Li, Y. Yang, Y. Li, *Nat. Commun.* **2016**, *7*, 10214.
- [40] W. Peng, L. Wang, B. Murali, K. T. Ho, A. Bera, N. Cho, C. F. Kang, V. M. Burlakov, J. Pan, L. Sinatra, C. Ma, W. Xu, D. Shi, E. Alarousu, A. Goriely, J. H. He, O. F. Mohammed, T. Wu, O. M. Bakr, *Adv. Mater.* **2016**, *28*, 3383.
- [41] Q. Dong, Y. Fang, Y. Shao, P. Mulligan, J. Qiu, L. Cao, J. Huang, *Science* **2015**, *347*, 967.